Journal of The Electrochemical Society, **148** (8) G434-G438 (2001)
0013-4651/2001/148(8)/G434/5/$7.00 © The Electrochemical Society, Inc.

Expanding the Process Window and Reducing the Optical Proximity Effect by Post-Exposure Delay

Chin-Yu Ku,[a] Jia-Min Shieh,[b] Tsann-Bim Chiou,[b] Hwang-Kuen Lin,[c] and Tan Fu Lei[a,z]

[a]*Department of Electronics Engineering and Institute of Electronics, National Chiao Tung University, Hsinchu 300, Taiwan*
[b]*National Nano Device Laboratories, Hsinchu 300, Taiwan*
[c]*Vanguard International Semiconductor Corporation, Hsinchu 300, Taiwan*

In this investigation, a novel idea had been proposed to expand the process window and reduce the optical proximity effect (OPE) by employing post-exposure delay (PED). Our previous work presented a model to specify the resist linewidth according to PED time based on the neutralization mechanism of organic base and photogenerated acid. Based on the model, the exposure latitude and depth of focus can be extended for various pattern sizes by applying PED on linewidth broadening. Moreover, the dense-iso critical dimension bias, which is caused by OPE, can also be reduced when PED is performed.
© 2001 The Electrochemical Society. [DOI: 10.1149/1.1383557] All rights reserved.

Manuscript received April 17, 2000. Available electronically July 10, 2001.

Modern high numerical aperture (NA) lithographic tools must accurately determine the best focus and tightly control dosage because both the depth of focus (DOF) and exposure latitude (EL) have decreased. Considerable effort has been made to stabilize the exposure condition and to more accurately measure the best focus and threshold energy (or "energy to clear," *i.e.,* the minimum required energy to remove photoresist) E_{th}, to maintain a safe process margin for mass production.[1-5] However, expanding the process window of the most critical linewidth, such as gate length, is the best way to solve this problem.

Airborne contaminants and linewidth changes with various delay times have continually plagued the deep ultraviolet (DUV) resists in the past. Significant effort has been expended to understand the role of each component in resist formation on lithographic performance to improve the process stability and resist performance.[6-17] Linewidth variation is primarily induced by the acid diffusion effect during the exposure and baking process. Therefore, the diffusion behavior of photogenerated acid has been widely investigated for both high and low activation energy (E_{a}) resist systems.[13-26] Base additives can reduce the linewidth slimming of low E_{a} systems such as acetal-based resists by reducing the acid diffusion.[12,22] Additional base components cannot only quench photogenerated acid, but can also suppress the acid diffusion reaction within the resist film.[13] Theoretical studies have also revealed that limited diffusion is the key factor in achieving high-resolution chemically amplified DUV resists.[27,28]

Our previous work investigated how an organic base additive affects the acid concentration and lithographic performance in *tert*-butoxycarbonyl (t-BOC) protected type chemically amplified positive DUV resist.[1] The resists included a t-BOC protected polystyrene base resin (substitution ratio around 25%) and an onium salt as a photoacid generator. A resist system composed of a chemically amplified positive resist and an organic base, such as NMP, not only prevents formation of a "T-top," but also suppresses the acid diffusion reaction within resist film.[13] The linewidth broadened immediately after exposure and then became a constant value instead of continuously expanding. A model was established to represent the linewidth variation behavior based on the organic base neutralization method. An equation was also derived to precisely specify the linewidth broadening behavior during PED for various pattern sizes. The EL and DOF can be extended for various isolated and dense patterns by employing the linewidth variation property caused by post-exposure delay.

Annular illumination was chosen for its improved resolution and DOF on dense lines. However, off-axis illumination (OAI) typically produces a larger dense-iso critical dimension (CD) bias and a reduced isolated line DOF compared to conventional illumination.[29] A novel approach to extend the EL and DOF as well as to reduce the dense-iso CD bias by employing post-exposure delay is developed herein. Moreover, PED can also significantly extend the common process window of isolated and dense patterns.

Background

Linewidth variation behavior during PED.—For a positive DUV resist, a radiation sensitive acid generator is decomposed during exposure and the subsequent acid-catalyzed thermal reaction is performed at an elevated temperature makes the resist soluble. A model that successfully describes the linewidth variation during PED for line-and-space dense patterns can also represent the concentration of activated acid as follows

$$[H^+(t)] = [H^+(0)] + [\mathrm{O}H^-(0)] \times \{\exp(-t/\tau) - 1\} \quad [1]$$

where $[H^+(t)]$ and $[\mathrm{OH}^-(t)]$ denote the concentration of activated acid and base after t minutes of PED, respectively. The constant τ in Eq. 1 stands for the time constant of the organic base. The space width $\mathrm{CD_s}(t)$ and $\mathrm{CD_s}(0)$ can be described by $[H^+(t)]$ and $[H^+(0)]$ because the acid distribution is defined by the aerial image of the resist. Equation 1 can be transformed to reveal the space width behavior during PED as follows

$$CD_{\mathrm{s}}(t) = CD_{\mathrm{s}}(0) + S[\exp(-t/\tau) - 1] \quad [2]$$

Table I. Maximum space width variation S for dense and isolated patterns.

Space width (μm)	S_{dense} (nm)	S_{iso} (nm)
0.18	13	38
0.20	12	37
0.22	14	36
0.25	20	37
0.30	23	39
0.35	28	40
0.40	29	40
0.45	30	37
0.50	30	39
0.60	27	39
0.70	25	38
0.80	25	36
0.90	26	39
1.00	29	40

[z] E-mail: tflei@cc.nctu.edu.tw

Downloaded on 2014-04-27 to IP 140.113.38.11 address. Redistribution subject to ECS terms of use (see ecsdl.org/site/terms_use) unless CC License in place (see abstract).

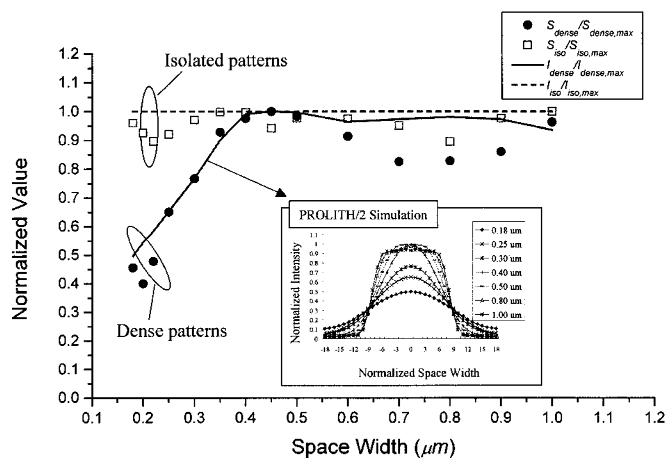

Figure 1. Normalized value of S_{ave} and normalized peak intensity.

Energy effect on space width variation.—the maximum space width deviation is represented by S in Eq. 2, which can be obtained by

$$S = CD_s(t = 0) - CD_s(t = \infty) \qquad [3]$$

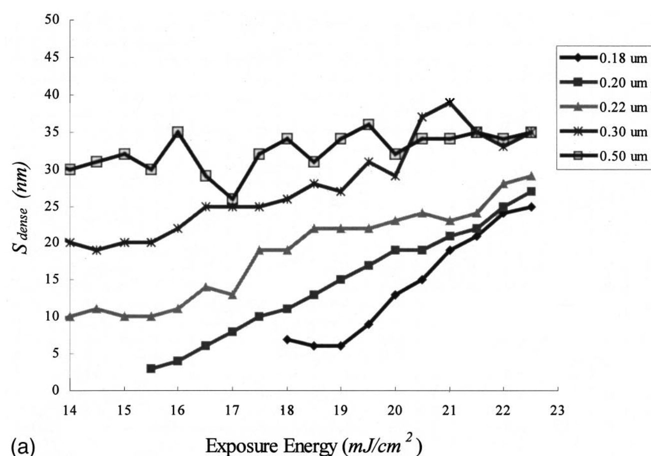

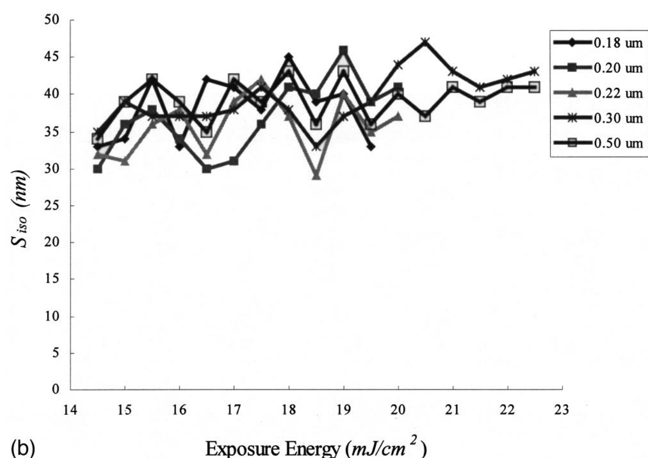

Figure 2. Maximum space width variation, S, for different space width at the energy level ranged from 14 to 22.5 mJ/cm^2. (a) Dense pattern. (b) Isolated patterns.

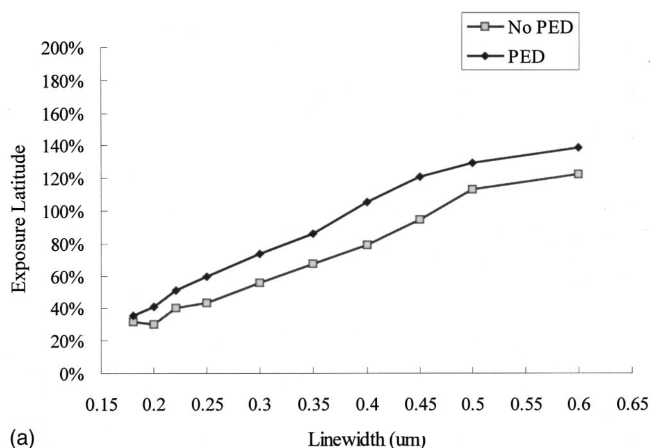

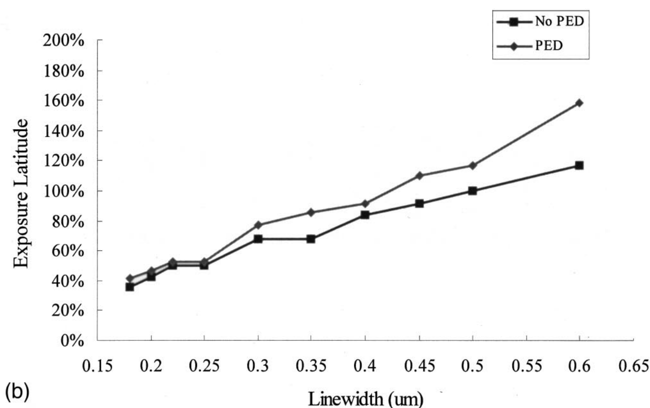

Figure 3. Energy latitude for various pattern sizes. (a) Dense patterns. (b) Isolated patterns.

The maximum space width variations S_{dense} and S_{iso} listed in Table I, were measured by a scanning electron microscope (SEM). The energy selection was based on the minimum mask bias for various pattern sizes. The linewidth variation was measured instead of the space width of isolated patterns to maximize efficiency. The largest S_{dense} was obtained when the mask size was 0.45 μm, and the value of $S_{dense,max}$ was 30 nm. Normalized $S_{dense}/S_{dense,max}$ and $I_{dense}/I_{dense,max}$ were employed to correlate the maximum space width variation and peak intensity as illustrated in Fig. 1. The intensity profile of dense patterns is also displayed in this figure according to the position of normalized space width. This aerial image profile was simulated via the PROLITH/2 modeling program.

The normalized space width variation ($S_{iso}/S_{iso,max}$) and normalized peak intensity for isolated lines ($I_{iso}/I_{iso,max} = 1$) are displayed in Fig. 1. The peak intensities are independent of the linewidth and remain nearly constant for various pattern sizes because the space width of isolated line patterns is presumed to increase infinitely. This model can be verified by comparing the experimental and theoretical results for dense and isolated patterns.

The energy dependence of the maximum space width variation for dense and isolated patterns are demonstrated in Fig. 2a and b. The maximum space width variation S_{dense} increases with the exposure energy when the space width is smaller than 0.5 μm. Figure 1 suggests that the acid concentration is much lower for a smaller space width, particularly when the space width is close to the exposure wavelength (248 nm). Therefore, higher exposure energy could create more photogenerated acid and increase the "effective" base concentration at the same time. Raising the exposure energy can largely increase the value of S_{dense} for smaller space widths because of the lower acid concentration as demonstrated in Fig. 2a.

Downloaded on 2014-04-27 to IP 140.113.38.11 address. Redistribution subject to ECS terms of use (see ecsdl.org/site/terms_use) unless CC License in place (see abstract).

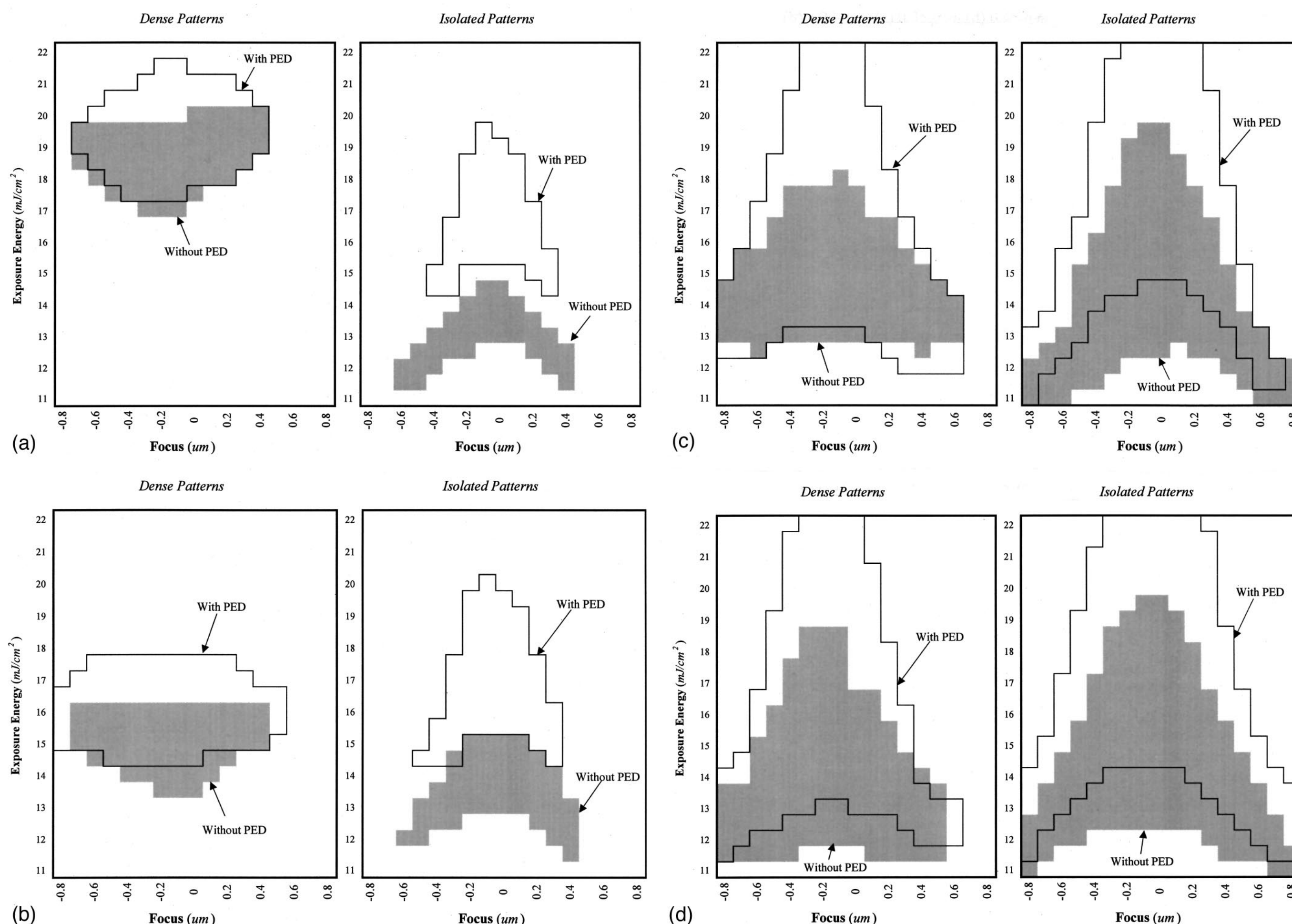

Figure 4. Process window with PED (defined by lines) and without PED (shaded area) of dense and isolated patterns, (a) 0.18, (b) 0.22, (c) 0.35, and (d) 0.45 μm.

The maximum linewidth variation presented in Fig. 2b is the difference between maximum linewidth and normal linewidth, *i.e.,* $CD_{\text{line}}(\infty) - CD_{\text{line}}(0) = CD_{\text{s}}(0) - CD_{\text{s}}(\infty) = S$. The isolated line is predicted to behave similarly to the larger dense patterns, such as 0.5 μm, because of the large space width for isolated patterns. Although the photogenerated acid neutralizes most of the added base, increasing the exposure energy can still raise the neutralization probability of the remaining active base. Therefore, a minor increase in maximum space width variation S along with exposure energy can be predicted for isolated and large line-and-space patterns as demonstrated in Fig. 2a and b.

Strategy to improve process window.—If the line-and-space patterns are exposed by two energy levels, E_1 and E_2 ($E_1 > E_2$), and the measured space widths are CD_1 and CD_2, respectively, the value of CD_1 is larger than that of CD_2 as a consequence of the higher exposure energy. The difference between the two space widths can be written as

$$\Delta CD = CD_1 - CD_2 > 0 \qquad [4]$$

when both patterns have a long-term post-exposure delay, the space widths are saturated and become constant. The value of S_1 is larger than the value of S_2, because the value of S is larger for the higher exposure energy when the space width variations are presumed to be S_1 for CD_1 and S_2 for CD_2. Therefore, the space width difference, which has a PED, between the two energy levels is

$$\Delta CD' = (CD_1 - S_1) - (CD_2 - S_2) = \Delta CD - (S_1 - S_2) < \Delta CD \qquad [5]$$

The space width is less sensitive to exposure energy when PED is performed because the value of $\Delta CD'$ is smaller than ΔCD. The effect of PED on EL and DOF is verified in the next section according to the energy dependence on the space width variation.

Experimental

Materials and processing.—The effect of an additional base component, *N*-methyl pyrrolidone (NMP), was investigated in *tert*-butoxycarbonyl (t-BOC) protected chemically amplified positive DUV resist. The resists included a t-BOC protected polystyrene base resin (substitution ratio around 25%) and an onium salt as a photoacid generator. The resist samples were coated on silicon substrates that were hexamethyl disilazane (HMDS) vapor primed. The positive DUV resist was spin-coated to 0.6 μm thickness and prebaked at 110°C for 90 s. All patterns were exposed by a KrF excimer laser scanner with a 0.63 NA lens and the post-exposure bake (PEB) was performed at 110°C for 90 s. The resist films were developed in a 2.38 wt % tetramethylammonium hydroxide (TMAH) based developer for 60 s. A Hitachi S-9200 SEM was used to measure the resist pattern linewidths. The ammonia concentration was controlled under 8 ppb by mol in the air and under 0.8 ppb by mol inside the track to prevent T-top formation.

Downloaded on 2014-04-27 to IP 140.113.38.11 address. Redistribution subject to ECS terms of use (see ecsdl.org/site/terms_use) unless CC License in place (see abstract).

Sample analyses.—Different pattern sizes were exposed and various delay time patterns were measured separately to investigate the effect of post-exposure delay between exposure and PEB. The measured lines or spaces studied herein included isolated and line-and-space dense patterns. The relationships between linewidth and PED time for various linewidths was determined through the measurement of pattern widths. The EL, DOF, and dense-iso CD bias were all determined from the focus exposure matrix (FEM).

Results and Discussion

PED affect on the exposure latitude and process window.—Equation 5 indicated that the linewidth decreased less in response to higher exposure energy if the PED is employed. Figures 3a and b present the EL of dense and isolated patterns. The exposure dose was optimized (E_{op}) to make the resist CD equal the mask CD. The EL is defined as the range with $\pm 10\%$ CD variation that is normalized by E_{op}. The EL was higher for both dense and isolated patterns, which concurs with our previous assumption.

Figures 4a-d depict the PED affect on the process windows for both dense and isolated patterns for 0.18, 0.22, 0.35, and 0.45 μm linewidths. The shaded area is the process window obtained from the normal condition (without PED), and the area defined by the lines is the process window realized under PED. Therefore, the process window can be expanded if PED is performed.

Process window evaluation of line-and-space dense patterns.—The allowed process window required higher exposure energy during PED because the linewidth broadened. The peak intensity of dense patterns will drop if the exposure is performed under the defocused situation. The previous equation confirms that the PED affects the measured linewidth more as the exposure energy is increased. Therefore, the allowed process region around the best focus point will have a larger shift than that of a defocused region. The process window under PED can almost cover the original process window for 0.18 and 0.22 μm line-and-space patterns because the value of S_{dense}, *i.e.,* the maximum CD deviation under PED, is less than 0.01 μm only if the linewidth is smaller than 0.22 μm as illustrated in Fig. 2a. Thus, the process window of PED can cover the no-PED window at lower energy level when the linewidth is "smaller."

The DOF may decrease if PED is employed due to the allowed process window shift around the best focus for the larger linewidth. For example, if 1 mJ/cm^2 is the required EL for mass production, the DOF of 0.45 μm dense patterns is 1.3 μm for normal condition but only 1.0 μm for PED condition. Fortunately, the deviation of "best focus region" and "defocus region" is minor for smaller linewidths and it does become until the linewidth is larger than 0.35 μm. The DOF of smaller linewidths is more significant because the larger linewidths have larger DOF. Therefore, employing PED can expand the process window for dense patterns since the impact of this deviation is not harmful for normal production.

Process window evaluation of isolated patterns.—The behavior of isolated patterns was evaluated after the performance of dense patterns was analyzed. The process window shifted to higher exposure energy level for the isolated patterns when PED was employed. Figures 2a and b demonstrate that the energy dependency of the isolated lines is similar to the larger dense lines, while Fig. 4a to b

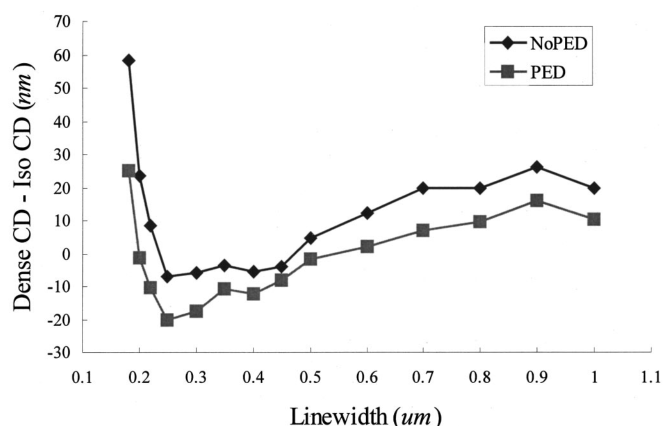

Figure 6. CD difference between dense and isolated patterns for various pattern sizes.

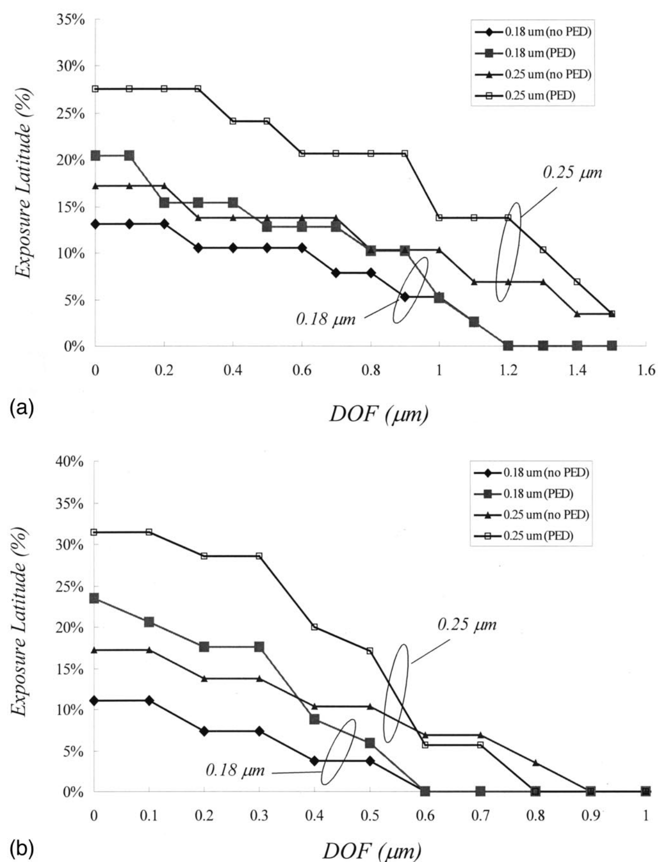

Figure 5. Exposure latitude of various DOF for 0.18 and 0.25 μm. (a) Dense patterns. (b) Isolated patterns (τ ranges from 8 to 11 min).

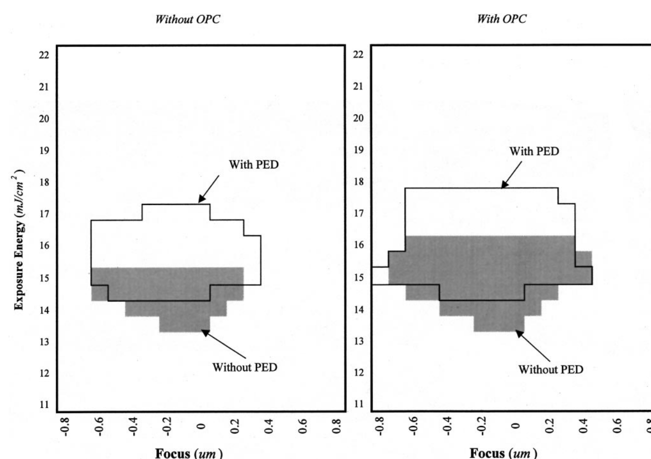

Figure 7. Comparison of common window (above 0.22 μm) between "without OPC" and "with OPC" for line-and-space dense patterns.

Downloaded on 2014-04-27 to IP 140.113.38.11 address. Redistribution subject to ECS terms of use (see ecsdl.org/site/terms_use) unless CC License in place (see abstract).

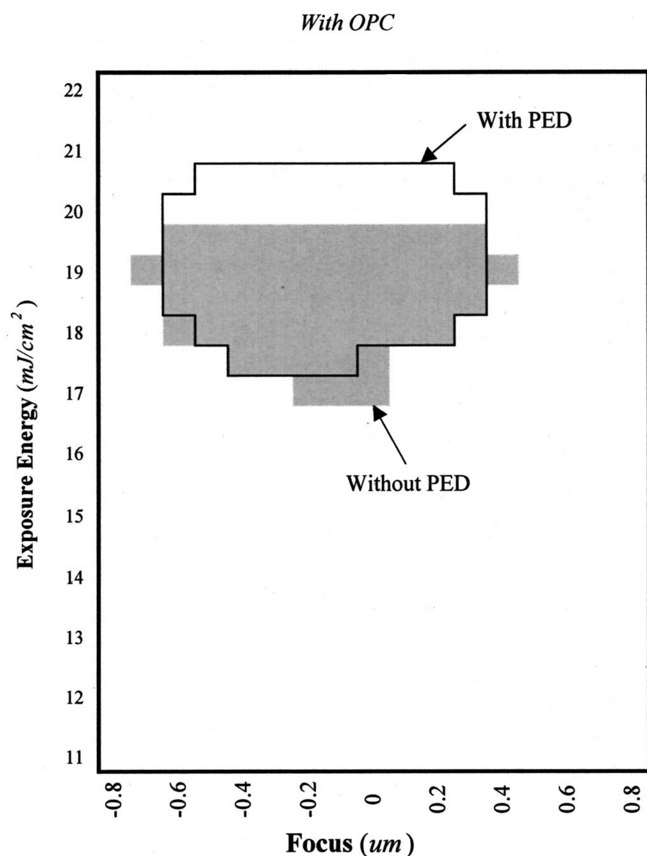

Figure 8. Common window (above 0.18 μm) under "normal" and "PED" for line-and-space dense patterns.

confirm that the shape of the allowed process windows of isolated patterns is similar to the result of larger dense patterns. The peak intensities are almost the same for both focused and defocused conditions because of the large space width of the isolated line. Therefore, the defocused region shifts more than the dense patterns. The common area between normal condition and PED condition is smaller because of the shifting of the process window, which concurs with our prediction. Figures 5a and b depict the plots of EL according to various DOF for dense and isolated patterns, respectively. The EL and DOF can be largely improved by PED for both 0.18 and 0.25 μm patterns.

PED affect on optical proximity effect.—The plots in Fig. 4a and b reveal that the process window of 0.18 and 0.2 μm isolated lines shifted to higher energy under PED. Therefore, the CD difference between dense and isolated patterns can be lowered if PED is utilized. The result in Fig. 6 can be determined by calculating the "dense-iso bias," which is almost 0.06 μm for 0.18 μm pattern under normal condition. The dense-iso bias can be reduced to 0.025 μm and there is almost no dense-iso bias for the 0.2 μm pattern when PED is performed. Although the dense-iso bias is smaller for the normal condition if the linewidth is between 0.25 and 0.45 μm, the maximum dense-iso bias under PED is still smaller than 0.02 μm.

The optical proximity correction (OPC) has been recently employed to not only reduce the dense-iso CD bias but also to correctly print various pattern sizes at the same time. The common process window between various linewidths can be extended by employing the properties of larger exposure latitudes (ELs) under PED. The optical proximity correction herein only changes the pattern widths on the mask (one-dimensional OPC). The process window of each linewidth is assumed to remain the same and only shifts along with the axis of exposure energy when the OPC is performed. Figure 7a presents the common window of 0.22, 0.25, 0.35, 0.45, and 0.7 μm dense patterns obtained without any optical proximity correction. The common process window of these patterns can be expanded if the OPC is applied as denoted in Fig. 7b. No common window exists if the 0.18 μm patterns are included in the previous condition because of the photoresist linearity. Therefore, OPC is necessary if the 0.18 μm pattern is simultaneously printed with other larger patterns. Figure 8 delineates the common window for 0.18 μm and larger linewidths if the optical proximity correction is applied. The process window can be further extended if PED is applied.

Conclusion

The exposure latitude and depth of focus can be expanded and a steady linewidth can be realized by employing a long term PED. The dense-iso CD bias, caused by the optical proximity effect, can also be reduced by a long term PED. The process window can be largely expanded for various pattern sizes when the long term PED are employed.

Acknowledgment

This work was supported by the National Science Council of R.O.C. under contract 88-2215-E009-045.

Dr. Lei assisted in meeting the publication costs of this article.

References

1. C. Y. Ku, J. M. Shieh, T. B. Chiou, H. K. Lin, and T. F. Lei, *J. Electrochem. Soc.,* **147**, 3833 (2000).
2. T. Itani, H. Yoshino, S. Hashimoto, M. Yamana, N. Samoto, and K. Kasama, *Photopolym. Photoimaging Sci. Technol.,* **10**, 409 (1997).
3. K. Suwa, H. Tateno, N. Irie, and S. Hirukawa, *Proc. SPIE,* **2440**, 712 (1995).
4. Y. C. Kim, G. S. Yeo, J. H. Lee, H. Kim, and U. I. Chung, *Proc. SPIE,* **3677**, 184 (1999).
5. R. R. Kunz, M. Y. Chan, and S. P. Doran, *Proc. SPIE,* **3679**, 108 (1999).
6. Y. Kawai, A. Otaka, A. Tanaka, and T. Matsuda, *Jpn. J. Appl. Phys., Part 1,* **33**, 7023 (1994).
7. S. A. MacDonald, N. J. Clecak, H. R. Wendt, C. G. Wilson, C. D. Snyder, C. J. Knors, N. B. Deyoe, J. G. Maltabes, J. R. Morrow, A. E. McGuire, and S. J. Holmes, *Proc. SPIE,* **1466**, 2 (1991).
8. T. Kumada, Y. Tanaka, A. Ueyama, S. Kubota, and H. Koezuka, *Proc. SPIE,* **1925**, 31 (1993).
9. A. Oikawa, N. Santoh, and S. Miyata, *Proc. SPIE,* **1925**, 92 (1993).
10. T. Fischer, U. Boettiger, A. Grassmann, H. Moritz, H. Binder, D. Funhoff, and R. Schwalm, *Microelectron. Eng.,* **23**, 311 (1994).
11. V. Deshpande, N. Thane, J. Hargreaves, Y. Takamori, and E. Apelgren, *Proc. SPIE,* **1926**, 208 (1993).
12. K. J. Przybilla, Y. Kinoshita, T. Kudo, S. Masuda, H. Okazaki, M. Padmanaban, G. Pawlowski, J. Roeschert, W. Spiess, and N. Suehiro, *Proc. SPIE,* **1925**, 76 (1993).
13. T. Itani, H. Yoshino, S. Hashimoto, M. Yamana, N. Samoto, and K. Kasama, *Microelectron. Eng.,* **35**, 149 (1997).
14. T. Itani, H. Iwasaki, M. Fujimoto, and K. Kasama, *Jpn. J. Appl. Phys., Part 1,* **33**, 7005 (1994).
15. T. Itani, H. Yoshino, S. Hashimoto, M. Yamana, N. Samoto, and K. Kasama, *Jpn. J. Appl. Phys., Part 1,* **35**, 6501 (1996).
16. T. H. Fedynyshyn, J. W. Thackeray, J. H. Georger, and M. D. Denison, *J. Vac. Sci. Technol. B,* **12**, 3888 (1994).
17. T. Itani, H. Yoshino, M. Fujimoto, and K. Kasama, *J. Vac. Sci. Technol. B,* **13**, 3026 (1995).
18. G. M. Wallraff, W. D. Hinsberg, F. A. Houle, M. Morrison, C. E. Larson, M. Sanchez, J. Hoffnagle, P. J. Brock, and G. Breyta, *Proc. SPIE,* **3678**, 138 (1999).
19. J. Kim, Y. Kwon, J. Choi, and M. Jung, *Proc. SPIE,* **3678**, 536 (1999).
20. J. L. P. Jessop, S. N. Goldie, A. B. Scranton, G. J. Blanchard, B. Rangarajan, L. Capodieci, R. Subramanian, and M. K. Templeton, *Proc. SPIE,* **3678**, 914 (1999).
21. X. Shi, *Proc. SPIE,* **3678**, 342 (1999).
22. L. Ferreira, S. Malik, T. R. Sarubb, A. J. Blakeney, and B. Maxwell, *Proc. SPIE,* **3333**, 236 (1998).
23. T. H. Fedynyshyn, C. R. Szmanda, R. F. Blacksmith, W. E. Houck, and J. C. Root, *J. Vac. Sci. Technol. B,* **11**, 2798 (1993).
24. G. Arthur, N. Eilbeck, and B. Martin, *Microelectron. Eng.,* **35**, 137 (1997).
25. D. J. H. Funhoff, H. Binder, and R. Schwalm, *Proc. SPIE,* **1672**, 46 (1992).
26. W. S. Huang, *Proc. SPIE,* **3678**, 1040 (1999).
27. J. Nakamura, H. Ban, and A. Tanaka, *Jpn. J. Appl. Phys., Part 1,* **31**, 4294 (1992).
28. T. Itani, H. Yoshino, S. Hashimoto, M. Yamana, N. Samoto, and K. Kasama, *Photopolym. Photoimaging Sci. Technol.,* **10**, 409 (1997).
29. P. Luehrmann, P. V. Oorschot, H. Jasper, S. Stalnaker, S. Brainerd, B. Rolfson, and L. Karklin, *Proc. SPIE,* **1927**, 103 (1993).

Downloaded on 2014-04-27 to IP 140.113.38.11 address. Redistribution subject to ECS terms of use (see ecsdl.org/site/terms_use) unless CC License in place (see abstract).